First-principle study on structural and electronic properties of CeO_2 and ThO_2 under high pressures

Hong X. Song, Lei Liu, Hua Y. Geng,* and Q. Wu

National Key Laboratory of Shock Wave and Detonation Physics, Institute of Fluid Physics, CAEP, P.O. Box 919-102, Mianyang, Sichuan, People's Republic of China, 621900

(Received 17 January 2013; revised manuscript received 15 April 2013; published 3 May 2013)

High-pressure structural and electronic properties of CeO_2 and ThO_2 are investigated with density functional calculations. An isostructural phase transition with space group *Pnma* at about 100 GPa has been observed in both compounds. The high-pressure *Pnma* phase is revealed as being an orthorhombic distortion of the hexagonal Ni_2In structure. A pressure-induced metallization in the high-pressure *Pnma* phase with a mechanism of Wilson transition is also predicted at around 250 GPa in CeO_2, and at 350 GPa in ThO_2, respectively. Two new metallic phases with space group $P\bar{3}m1$ and $I4/mmm$ are found as the ground state in CeO_2 when pressure is above 450 GPa, whereas in ThO_2 the *Pnma* phase is stable up to 1 TPa. The equations of state are analyzed, as well as the pressure dependence of the lattice parameters, atomic fractional coordinates, and electronic band gaps.

DOI: 10.1103/PhysRevB.87.184103 PACS number(s): 61.50.Ks, 71.15.Mb, 71.20.−b, 91.60.Gf

I. INTRODUCTION

Ceria (CeO_2) and thoria (ThO_2) are two important technical materials. CeO_2 is widely used as automobile exhaust catalyst, electrolyte of solid oxide fuel cell, and oxygen storage device, etc. ThO_2 has less industrial applications because of its radioactivity, but has also attracted a great deal of interest due to its potential as the next generation nuclear reactor fuel. A considerable number of studies have been performed on their physical and chemical properties with experimental and theoretical methods. Most of the published works have focused mainly on properties at ambient conditions. However, a thorough understanding of the structural and electronic properties under high pressures is important not only for fundamental physics, but also for issues relating to technology and industry.

Since elements Ce and Th belong to the same column in the periodical table, their dioxides exhibit similarities in many structural and electronic properties. Both of them crystalize in a cubic fluorite phase [space group $Fm\bar{3}m$, with four formulas in a unit cell ($Z = 4$)] under ambient conditions, which transforms to an orthorhombic cotunnite phase (space group *Pnma*, $Z = 4$) at high pressures.[1–5] In the fluorite phase, the lattice parameters, bulk moduli, elastic constants, and phonon dispersion relations of these compounds are also very close.[6] From the electronic viewpoint, they have similar valence configurations and bonding features. By donating four electrons to two oxygen atoms, each metal cation is nominally tetravalent.[7,8] The charge transfer from one Ce or Th cation to two O anions makes the localized f state unoccupied, and thus the strong correlation effect is far less important than in their sesquioxides.[9,10] The electronic band structures of CeO_2 and ThO_2 are similar, excepting the presence of the empty $4f$ band between the $2p$ valence band and the $5d$ conduction band in CeO_2.[6] Both of these two compounds are insulators, with a fundamental band gap (p-d gap) about 6 eV (Refs. 11 and 12). At higher pressures, however, the gap will close due to band overlapping driven by compressions, thus we can expect a pressure-induced metallization in both CeO_2 and ThO_2.

Since structural stability is a fundamental property, it is worth mentioning more details about the high-pressure structures. Experimentally, the fluorite-cotunnite transition has been well studied. In CeO_2, the high-pressure cotunnite phase has been observed with both x-ray diffraction (XRD)[2] and Raman[1] experiments. However, the low resolution of the early energy dispersive x-ray diffraction (EDXD) failed to give any information on the Wyckoff positions of atoms. This structural transition was also observed in nanocrystal CeO_2 (Refs. 13 and 14). Due to effect of particle size, the transition pressure (22.3–26.5 GPa) is lower than the bulk sample (31 GPa). Interestingly, a metastable phase was recovered from the cotunnite phase of nanosized CeO_2, which was assigned as a hexagonal structure with 16 formulas in a unit cell ($Z = 16$).[13] On the other hand, the cotunnite phase is stable up to 70 GPa,[2] the highest pressure investigated in CeO_2 so far. For ThO_2, early EDXD[4] and Raman[3] experiments have also observed the high-pressure cotunnite phase, however, there is some inconsistency on the transition pressure. Recently, Idiri *et al.* studied its high-pressure behavior up to 80 GPa using an angle dispersive x-ray diffraction (ADXD) technique.[5] They found that the fluorite-cotunnite transition begins at around 33 GPa, which is close to the result of Raman experiment.[3] The observed transition pressure in ThO_2 is similar to CeO_2 but more sluggish (33–49 GPa). A Rietveld refinement of the XRD pattern was also performed to acquire the atomic coordinates.[5] Up to now, there is no experimental report for ThO_2 beyond 80 GPa in literature.

Theoretically, the fluorite-cotunnite transition has already been investigated by total-energy calculations within density functional theory (DFT) both in CeO_2 (Ref. 15) and ThO_2.[16–18] Remarkably, Wang *et al.* observed an isostructural transition from cotunnite phase to another *Pnma* phase in ThO_2 with a transition zone between 80 and 130 GPa.[18] This isostructural transition in *Pnma* phase was noticed and studied by Geng *et al.* in UO_2.[19] Within the isostructural transition zone, there is an abnormal variation of the lattice parameters, and the compressional behavior in the postcotunnite phase is also quite different from the cotunnite phase.

Despite these studies, our knowledge on the structural and electronic behaviors of these compounds above megabar pressures is still insufficient. To our knowledge, there is no report on postcotunnite phases in CeO_2 either theoretically or experimentally. The structural and electronic properties of

CeO_2 and ThO_2 beyond the cotunnite phase are still poorly understood. The possible pressure-induced metallization in these two compounds is completely unknown, not to mention the underlying mechanism. In this paper, we have investigated the structural and electronic properties of CeO_2 and ThO_2 above megabar pressures with DFT calculations. The long-standing issues mentioned above are addressed. Since CeO_2 and ThO_2 are typical dioxide of light-lanthanides and light-actinides, respectively, their high-pressure behaviors have a far-reaching impact on understanding the physical properties of other members in these series. The remainder of the paper is organized as follows. In Sec. II we describe our computational method. In Sec. III, the results and discussion are presented. Finally in Sec. IV, we conclude the main findings.

II. COMPUTATIONAL DETAILS

All of the properties reported here are calculated with the density functional theory,[20,21] as implemented in the plane-wave based VASP code.[22,23] The Perdew-Burke-Ernzerhof (PBE) version[24] of the general gradient approximation (GGA) is used for the electron exchange-correlation functional. Electrons of $5s^25p^64f^26s^2$ for cerium, $6s^26p^66d^27s^2$ for thorium, and $2s^22p^4$ for oxygen are treated as valence configurations. The interaction between the valence electrons and the remaining core electrons is described by the frozen core projector-augmented wave (PAW) method.[25,26] All calculations are spin polarized, though the ground states are nonmagnetic. All structural degrees of freedom that cannot be fixed by symmetry are fully relaxed at fixed volumes, with an electronic self-consistency convergence of 10^{-6} eV, and a Hellmann-Feynman force tolerance of 2×10^{-3} eV/Å. Integrations over the reciprocal space are performed using the smearing scheme of tetrahedron method with Blöchl corrections.[27] For Brillouin-zone sampling, the Monkhorst-Pack scheme[28] is employed. There are at least 18 nonequivalent k points in the irreducible Brillouin zone for the cubic fluorite phase, and more than 36 nonequivalent k points for cotunnite and other noncubic phases. The kinetic energy cutoff for the plane-wave basis set is 500 eV. The above parameters ensure that all the calculated total energies are converged to a level of 1 meV per atom.

As mentioned above, the oxidation state of the metal cations in CeO_2 and ThO_2 are nominally tetravalent. Because none of the localized $4f$- or $5f$-like band is occupied, the plain DFT method is enough to describe the ground-state structural and electronic properties.[6,9,10,18,29–31] It is therefore unnecessary to employ other sophisticated methods, such as hybrid functionals,[9,32,33] self-interaction corrected local spin density (SIC-LSD) approximation,[8] or DFT with Hubbard U (DFT + U) methods.[6,9,10,34–37] It has been demonstrated that the improvements of these sophisticated methods are mainly on the empty f levels, and the influence on the structural and electronic properties is insignificant.[6,10,38] However, to ensure the results being reliable, some PBE + U calculations are also performed. In these PBE + U calculations, a rotationally invariant version[39] is employed to account for the interaction among f electrons, with the semiempirical parameters U = 6 eV, J = 0.5 eV for CeO_2 and U = 4.5 eV, J = 0.5 eV for ThO_2. We found that there is no qualitative difference between PBE and PBE + U results on the structural and electronic properties presented below. In the following text, results without any special notation are all calculated with the standard DFT framework.

We also searched stable and metastable phases beyond the cotunnite phase with an evolutionary method using particle swarm optimization (PSO) algorithm as implemented in the CALYPSO code.[40] The simulation was performed at a fixed pressure of P = 100, 110, 120, 150, 200, 300, 350, 500, and 1000 GPa, respectively. The volume of the simulated supercell is variable, and the number of formulas per cell varies from 1 to 16.

III. RESULTS AND DISCUSSION

A. Structural properties

Recently we have found two postcotunnite phases (space group $Cmc2_1$ and $Cmcm$, both $Z = 4$) in UO_2 and PuO_2 above 120 GPa.[41] These two orthorhombic phases are distortions of a hexagonal Ni_2In phase (space group $P6_3/mmc$, $Z = 2$), which is a typical structure in binary compounds with chemical constitution of AX_2 or A_2X. However, all of these structures were found having higher enthalpy than the $Pnma$ phase in CeO_2 and ThO_2 where the f orbitals are unoccupied, indicating the crucial role played by f electrons in structure evolutions of heavy metal compounds along compressions.

In particular, our structural search did not find any structure that is more stable than the $Pnma$ phase within 1 TPa for ThO_2. However, a trigonal structure with space group $P\bar{3}m1$ ($Z = 2$) at around 500 GPa and a body-centered-tetragonal structure with space group $I4/mmm$ ($Z = 2$) at around 1 TPa were found being preferred in energy for CeO_2. Figure 1 depicts the crystal structures of these two high-pressure phases of CeO_2, and Fig. 2 shows the calculated enthalpy differences with PBE functional. Under compressions, the $Pnma$ phase first transforms into the $P\bar{3}m1$ phase at 458 GPa, then changes to $I4/mmm$ phase at 805 GPa. This relative order of phase stability is also confirmed by our PBE + U calculations. It is necessary to point out that both the $P\bar{3}m1$ and $I4/mmm$ phases are unfavored in ThO_2, though the enthalpy difference between $P\bar{3}m1$ and $Pnma$ reaches a value as small as 8 meV

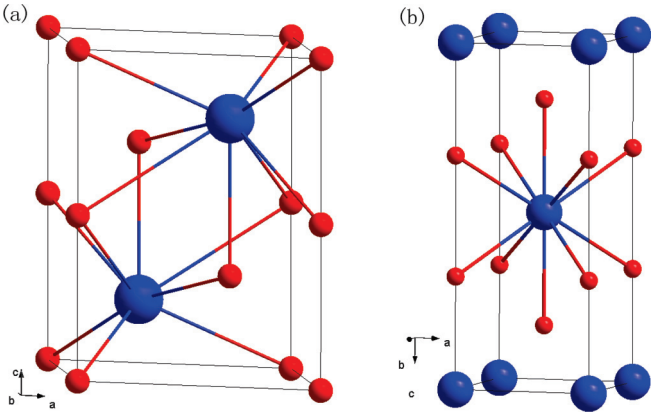

FIG. 1. (Color online) Crystal structures of the high-pressure (a) $P\bar{3}m1$ and (b) $I4/mmm$ phases observed in CeO_2. Blue large spheres are cerium cations and red small ones are oxygen anions.

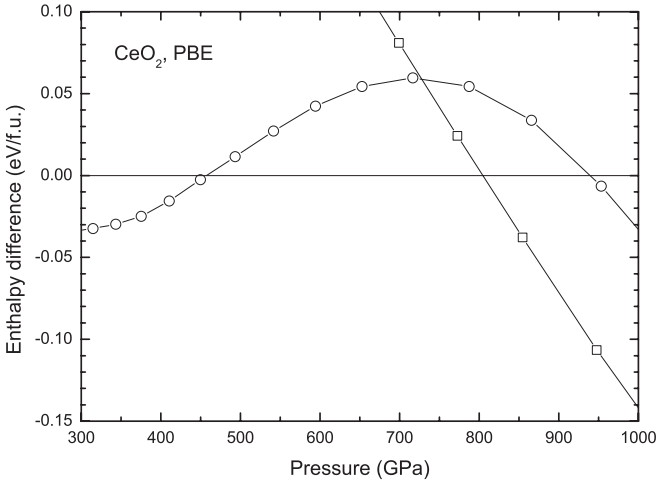

FIG. 2. The PBE calculated enthalpy differences of *Pnma* (open circles), $P\bar{3}m1$ (solid line), and $I4/mmm$ (open squares) phases in CeO_2 at high pressures. The $P\bar{3}m1$ phase is set as the zero reference.

per formula unit at around 420 GPa. This different behavior between CeO_2 and ThO_2 might be due to the different size of the cation cores, which affects the packing pattern of atoms under high compressions. In Fig. 3, we exhibit the variation of the lattice ratio c/b of the *Pnma* phases in CeO_2 and ThO_2. It can be seen that the lattice ratio of c/b in ThO_2 is smaller than 1.75 at around 400 GPa, which becomes less than $\sqrt{3}$ when above 500 GPa. This reorganization in the orthorhombic *Pnma* phase of ThO_2 makes itself more preferable in energy than the trigonal $P\bar{3}m1$ phase. Comparing to ThO_2, the ratio c/b in CeO_2 keeps almost constant at about 1.75 within a wide pressure range until 850 GPa, and is higher than that of ThO_2 even beyond 1 TPa. Such a difference in packing of atoms is echoed by the relative phase stability among the *Pnma*, $P\bar{3}m1$, and $I4/mmm$ structures in CeO_2 and ThO_2. In the $P\bar{3}m1$ structure of CeO_2, the occupied Wyckoff sites are $2d(\frac{1}{3}, \frac{2}{3}, z)$ for Ce, $1a(0, 0, 0)$ for O1, $1b(0, 0, \frac{1}{2})$ for O2, and $2d(\frac{1}{3}, \frac{2}{3}, z)$ for O3. Similar to the $Cmc2_1$

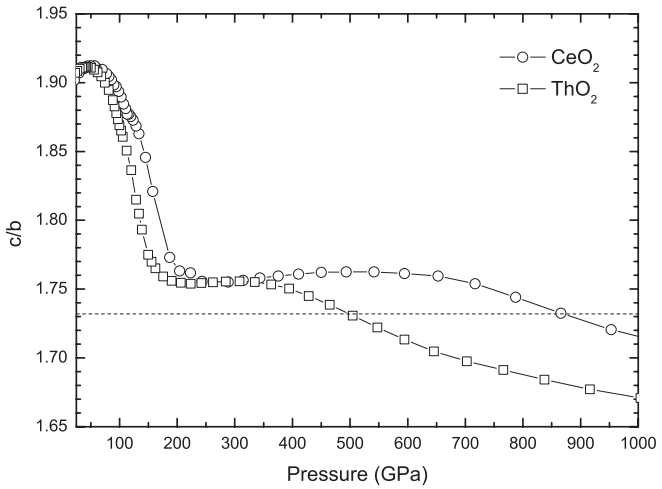

FIG. 3. Lattice ratio of c/b of the *Pnma* phases in CeO_2 and ThO_2 up to 1 TPa. Note that the *Pnma* phase in CeO_2 is metastable above 458 GPa.

and *Cmcm* phases in UO_2 and PuO_2, this phase is also a distorted-Ni_2In structure: the internal parameters z(Ce) and z(O3) in $P\bar{3}m1$ deviate from that of $\frac{1}{4}$ and $\frac{3}{4}$ in $P6_3/mmc$. From a viewpoint of symmetry, both space group $P\bar{3}m1$ and *Cmcm* are maximal *translationengleiche* subgroups of $P6_3/mmc$,[42,43] i.e., the complete translational symmetries are preserved in the subgroups. We would like to point out that the $P\bar{3}m1$ phase could be derived from the *A*-type structure of Ce_2O_3, with adding four additional oxygen atoms at the middle of the *c* edges (the $1b$ Wyckoff site). For the $I4/mmm$ phase, the occupied Wyckoff sites are $2a(0, 0, 0)$ for Ce, and $4e(0, 0, z)$ for O. This ultrahigh-pressure tetragonal phase seems having no direct relationship with $P6_3/mmc$. But interestingly, it could be related to the ground-state cubic fluorite phase. In terms of symmetry, space group $I4/mmm$ is also one maximal *translationengleiche* subgroup of $Fm\bar{3}m$.[42,43] The calculated lattice parameters and atomic fractional coordinates of the $P\bar{3}m1$ and $I4/mmm$ phases at selected pressures are listed in Table I.

According to our PBE calculations, the *Pnma* phase is stable up to 458 GPa in CeO_2 and at least 1 TPa in ThO_2, respectively. Figures 4 and 5 illustrate the pressure dependence of the lattice parameters and atomic fractional coordinates in CeO_2 and ThO_2, respectively. The isostructural transition zone between 80 and 130 GPa in ThO_2 (Ref. 18) was verified. In CeO_2, this transition zone locates between 106 and 160 GPa, which is about 30 GPa higher than that of ThO_2,[18] UO_2,[19,41] and PuO_2.[41,44] Determination of the transition zones shown in Figs. 4 and 5 is based on analysis of lattice parameters, internal atomic coordinates, bond lengths, and coordination number. As can be seen in Fig. 3, the transition zone also corresponds to a region in which the lattice ratio c/b drops from about 1.9 to around 1.75. In the transition zone, the middle *a* axis drastically decreases, while the shortest *b* axis and the longest *c* axis increase slightly. The compressional variation of the rebounded *b* and *c* axes is also different in the transition zone.

The evolution of these structural parameters indicates that the *Pnma* phase above megabar pressures (i.e., that after the transition zone, hereafter referred to as HP-*Pnma* phase) is not the same as the low-pressure one (the cotunnite phase, referred to as LP-*Pnma* phase), in spite of the fact that they belong to the same space group. As illustrated in Figs. 4(a) and 5(a), the compressibility in the HP-*Pnma* phase is close to being isotropic rather than anisotropic as in the standard low-pressure cotunnite phase. The fact that $c/b \approx \sqrt{3}$ (see Fig. 3) also reveals that the HP-*Pnma* phase is an orthorhombic distortion of the hexagonal Ni_2In phase. In the *Pnma* structure, all cations (Ce/Th) and anions (O1 and O2) occupy the $4c$ $(x, \frac{1}{4}, z)$ Wyckoff sites. In the $P6_3/mmc$ structure, anions are sitting in two nonequivalent sites: $2a$ (0,0,0) for O1 and $2c$ $(\frac{1}{3}, \frac{2}{3}, \frac{1}{4})$ for O2, while the cations occupy the $2d$ $(\frac{1}{3}, \frac{2}{3}, \frac{3}{4})$ site. Since space group *Pnma* is also a subgroup of $P6_3/mmc$, the hexagonal structure could also be described in an orthorhombic setting. In other words, a configuration of *Pnma* structure with $c/b = \sqrt{3}$ and atomic occupation of z(Ce/Th) = z(O1) = $\frac{11}{12}$, x(O1) = $\frac{3}{4}$, x(Ce/Th) = z(O2) = $\frac{1}{4}$, x(O2) = 0 is equivalent to a volume doubled supercell of $P6_3/mmc$ structure. As illustrated in Figs. 4 and 5, the HP-*Pnma* phase in CeO_2 and ThO_2 has a close relationship with the hexagonal Ni_2In

TABLE I. Calculated lattice parameters and atomic fractional coordinates of the $P\bar{3}m1$ and $I4/mmm$ phases in CeO_2 at selected pressures.

Phase (space group no.)	Pressure (GPa)	Lattice parameters (Å, °)			Atomic coordinates (fractional)			
$P\bar{3}m1$	540	$a = 3.214$	$b = 3.214$	$c = 4.025$	Ce	0.3333	0.6667	0.2118
(164)		$\alpha = 90.00$	$\beta = 90.00$	$\gamma = 120.00$	O1	0.0000	0.0000	0.0000
					O2	0.0000	0.0000	0.5000
					O3	0.3333	0.6667	0.6866
$I4/mmm$	850	$a = 2.321$	$b = 2.321$	$c = 5.754$	Ce	0.0000	0.0000	0.0000
(139)		$\alpha = 90.00$	$\beta = 90.00$	$\gamma = 90.00$	O	0.0000	0.0000	0.3256

structure, namely, an orthorhombic distortion of the latter. The major differences between them are x(Ce/Th) and x(O1) deviate from the ideal values of $\frac{1}{4}$ and $\frac{3}{4}$, respectively. Other minor distortions include the following: the b axis of the *Pnma* structure is slightly shorter than the corresponding axis of the $P6_3/mmc$ structure, and the atomic fractional coordinate x(O2) also deviates a little bit. In ThO_2, the coordinates of z(Th) and z(O1) also do not converge to $\frac{11}{12}$ perfectly. In general, the structural behaviors of CeO_2 and ThO_2 are very similar within 450 GPa. The HP-*Pnma* phase is an orthorhombic distortion of the hexagonal Ni_2In-type $P6_3/mmc$ structure, which is compatible with other two orthorhombic distortions ($Cmc2_1$ and $Cmcm$) observed in UO_2 and PuO_2.[41] In this perspective, the isotropic compressibility of the HP-*Pnma* phase could be easily understood by realignment of the oxygen trigonal prisms along the a axis.[41]

To aid experimental detection of the isostructural transition within *Pnma*, we have simulated the corresponding XRD patterns. The results of CeO_2 at selected pressures are illustrated in Fig. 6. The patterns of ThO_2 are similar and not shown here. The ideal $P6_3/mmc$ structure is also plotted to show how far the HP-*Pnma* phase distorts from it. As demonstrated in Fig. 6, rearrangement of atoms in the HP-*Pnma* phase makes its XRD pattern totally different from the LP-*Pnma* phase. Instead, it is more close to that of the hexagonal Ni_2In phase. If the major peaks merge and minor peaks disappear, the HP-*Pnma* phase will completely degenerate into the nondistorted $P6_3/mmc$ structure.

Table II gives the bond lengths of the LP-*Pnma* and HP-*Pnma* phases in CeO_2 and ThO_2, at several selected pressures. We can see that the coordination number of cations increases from 9 (4 + 5) in the low-pressure cotunnite phase (CN = 9) to 11 (5 + 6) in the isostructural HP-*Pnma* phase (CN = 11). Interestingly, this isostructural transition within space group *Pnma* was also observed in cesium sulphide (Cs_2S) at 1–5 GPa, in which the evolution of bond lengths and coordination number are very similar.[45] Within the transition zone, the *Pnma* structure is 10 coordinated (5 + 5, CN = 10),

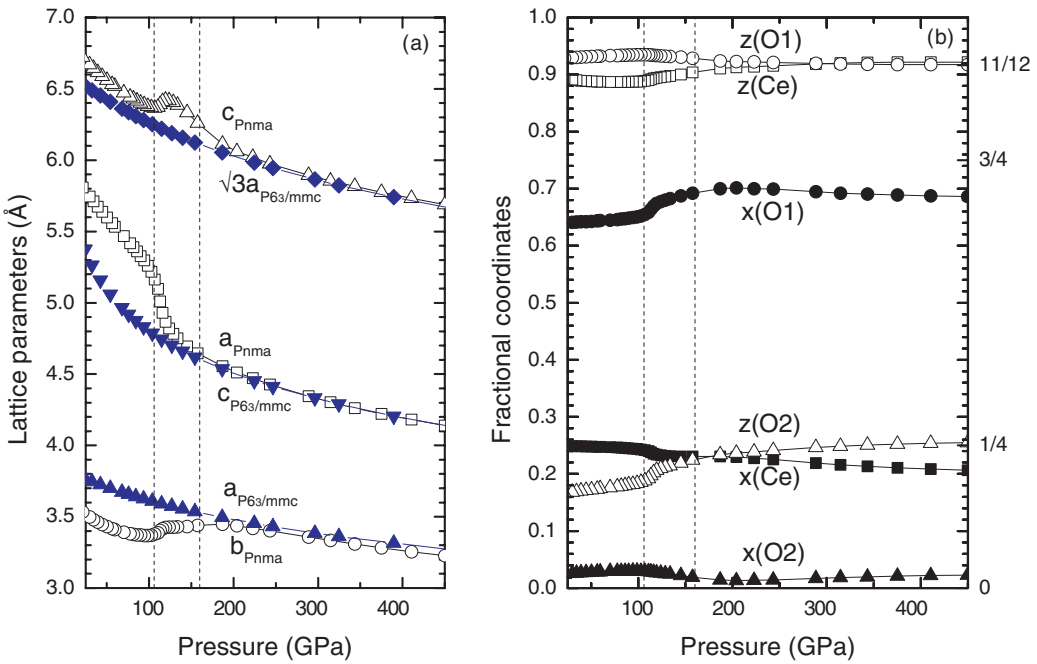

FIG. 4. (Color online) Variation of (a) lattice parameters and (b) fractional coordinates with pressure for CeO_2. In order to illustrate how *Pnma* [black open symbols in (a)] distorts from the $P6_3/mmc$ phase, the lattice parameters of the latter phase [blue solid symbols in (a)] are plotted. The ideal positions [labels at the right scale of (b)] when *Pnma* [solid and open symbols in (b)] continuously transforms to $P6_3/mmc$ are also given. Dashed vertical lines denote the boundary of the isostructural transition zone.

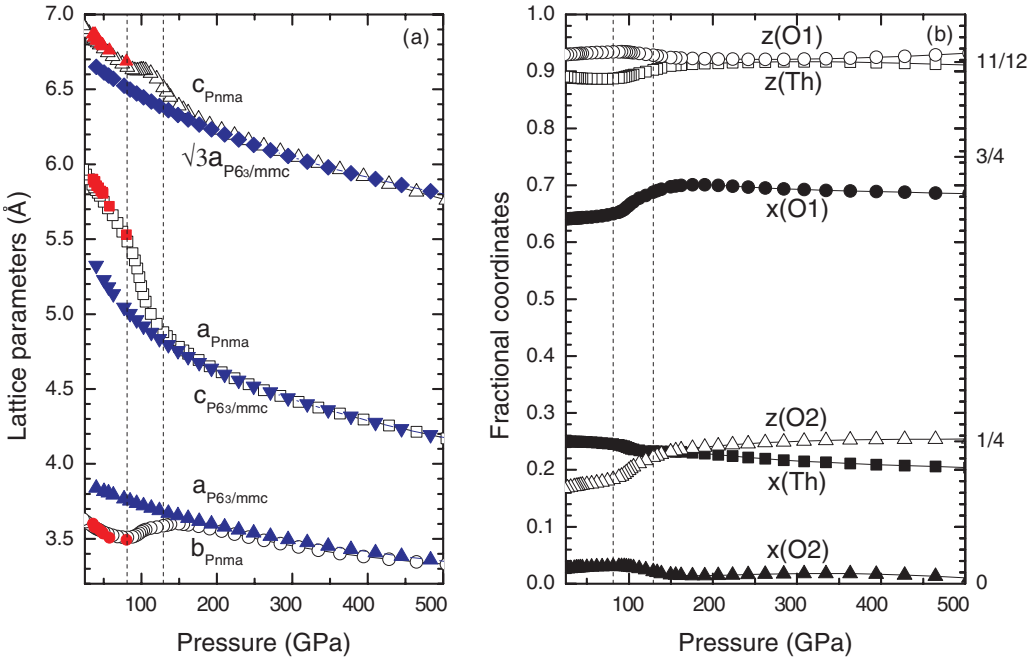

FIG. 5. (Color online) Variation of (a) lattice parameters and (b) fractional coordinates with pressure for ThO_2. Symbols are the same as Fig. 4. Red solid symbols in (a) are available experimental lattice parameters of the cotunnite phase (Ref. 5).

both in CeO_2 and ThO_2. As mentioned above, the $P\bar{3}m1$ phase in CeO_2 is a trigonal distortion of the $P6_3/mmc$ structure, therefore it is also 11 coordinated. Generally speaking, atoms tend to increase their coordination number and prefer to adopt denser structures under high pressures, which is well known as the "pressure coordination rule." This law is obeyed in the phase-transition sequences of CeO_2 and ThO_2, until the transformation into the $I4/mmm$ structure in CeO_2. The layered $I4/mmm$ structure is 10 coordinated (CN = 10), and its bond lengths are also remarkable: the nearest O-O distance is 1.86 Å at around 850 GPa, which is smaller than the nearest Ce-O distance (1.87 Å).

The above investigations extend a series of theoretical studies on high-pressure structural behaviors of actinide dioxides, in which there is always an isostructural transition zone around 80–130 GPa.[18,19,41,44] This isostructural transition was carefully reassessed in this work. We confirmed that the postcotunnite phases in actinide dioxides and lanthanide

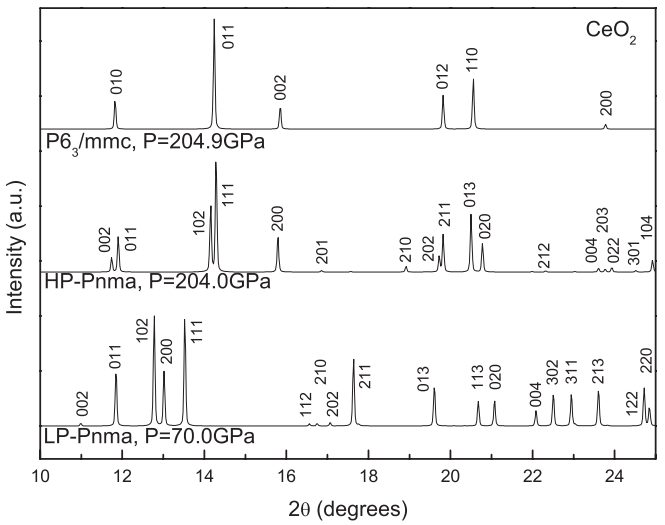

FIG. 6. Simulated XRD patterns of the low-pressure cotunnite phase (LP-*Pnma*, bottom pattern), the isostructural high-pressure phase (HP-*Pnma*, middle pattern), and the idea Ni_2In phase ($P6_3/mmc$, top pattern) in CeO_2. A monochromatic synchrotron radiation with wavelength of $\lambda = 0.6199$ Å was used. Numbers in parentheses label their (hkl) reflections.

TABLE II. Calculated bond lengths (Å) for CeO_2 and ThO_2 at selected pressures.

CeO_2	LP-*Pnma* (70 GPa)	HP-*Pnma* (204 GPa)
Ce-O1	2 × 2.14	2 × 2.01
	1 × 2.15	1 × 2.04
	1 × 2.20	1 × 2.13
		1 × 2.38
Ce-O2	1 × 2.22	1 × 2.19
	2 × 2.31	2 × 2.23
	2 × 2.50	2 × 2.33
		1 × 2.48
ThO_2	LP-*Pnma* (68.1 GPa)	HP-*Pnma* (206.2 GPa)
Th-O1	2 × 2.21	2 × 2.08
	1 × 2.22	1 × 2.10
	1 × 2.26	1 × 2.18
		1 × 2.43
Th-O2	1 × 2.30	1 × 2.26
	2 × 2.39	2 × 2.31
	2 × 2.57	2 × 2.39
		1 × 2.52

dioxides have a close relationship with the hexagonal Ni_2In structure. Although the hexagonal Ni_2In phase is energetically favored in neither of them, all of the predicted postcotunnite phases are its orthorhombic distortions, i.e., the $Cmc2_1$ distortion in UO_2, $Cmcm$ distortion in PuO_2, and $Pnma$ distortion in CeO_2 and ThO_2. Unlike UO_2 and PuO_2,[41] the internal parameters x(Ce/Th) and x(O1) of the HP-$Pnma$ phase in CeO_2 and ThO_2 deviate from the ideal positions of $\frac{1}{4}$ and $\frac{3}{4}$ more significantly. This difference might have nothing to do with the size effect of the ionic cores, because the calculated ground-state cation-anion radius ratio r_c/r_a with Bader's definition[46–48] is 1.07 (1.11) for CeO_2 (ThO_2), which is comparable to 1.12 (1.11) for UO_2 (PuO_2).[41] The variation of this ratio under high pressures is also very similar for these four compounds. Anyway, further investigations are required in order to confirm the underlying mechanism that hinders the HP-$Pnma$ phase in CeO_2 or ThO_2 from transforming into the more isotropic $P6_3/mmc$ structure. The underlying physical mechanism of the various post-$Pnma$ phases in these compounds remains unclear. This topic is, however, beyond the scope of this paper.

B. Equations of state

The equation of state (EOS) for CeO_2 at zero Kelvin was calculated up to 1 TPa and shown in Fig. 7. For ThO_2, it is identical from that of Ref. 18 and not presented here. There are kinks or discontinuities in EOS within the isostructural transition zones of these two compounds, similar to that in UO_2 and PuO_2.[41] It is also worth mentioning that these kinks or discontinuities are more noticeable in P-V curves than in E-V curves, which clearly demonstrates that the transition belongs to the first order.

From Fig. 7 it can be seen that the overall agreement between our calculations and the available experimental data is satisfactory. The small deviations in compressibility and phase-transition pressures could be attributed to the nonhydrostatic conditions[2,13] and the surface effect of the nanosized samples[13] used in experiments. Our calculated EOS for the fluorite phase of CeO_2 is consistent with the hydrostatic experiments,[49] as well as a recent hydrostatic correction to nonhydrostatic experiments.[50] The volume collapse when transforming from the fluorite to cotunnite phase is about 6%, which is comparable with the experimental values of $7.5\% \pm 0.7\%$ in the bulk sample[2] and 9.4% in the nano sample.[13] On the other hand, the volume changes in transitions from HP-$Pnma$ to $P\bar{3}m1$ and then to $I4/mmm$ are rather small (less than 1%). In Fig. 7, we also compare the EOS for the fluorite and cotunnite phases calculated with PBE functional and that of PBE + U. It is evident that the inclusion of the Hubbard corrections on localized f orbitals has little improvement on the EOS of both CeO_2 and ThO_2, which is reasonable since none of these f orbitals is occupied.

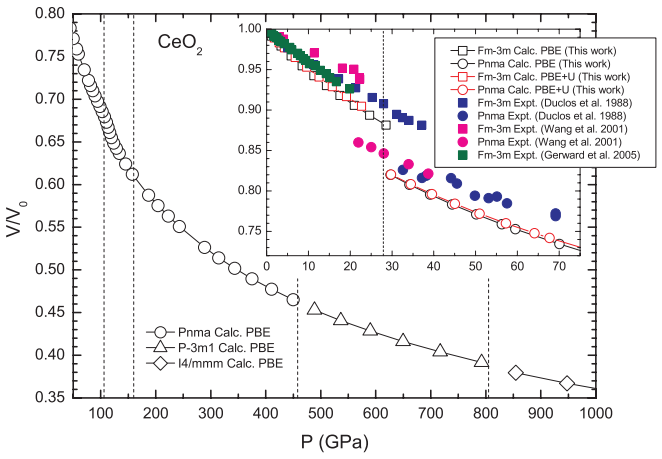

FIG. 7. (Color online) Equation of state for CeO_2 up to 1 TPa. Dashed lines denote the calculated phase-transition pressures with PBE functional. Inset shows the calculated EOS of the low-pressure fluorite and cotunnite phases, together with available experimental data for bulk (Refs. 2 and 49) and nano (Ref. 13) samples. The results of PBE + U calculations for the fluorite and cotunnite phases are also shown.

C. Electronic properties

CeO_2 and ThO_2 are large-gap insulators at ambient conditions. The experimental fundamental gap between the occupied O-2p valence band and the unoccupied Ce-5d or Th-6d conduction band is about 6 eV.[11,12] In CeO_2, the band gap between the O-2p valence band and the empty Ce-4f band is about 3 eV (Ref. 11). In ThO_2, electronic density of states (DOS) shows that the unoccupied Th-5f orbital is merged into the Th-6d state in the conduction band.[6,18] Our calculated 2p-4f (2p-5d) band gaps of CeO_2 are 1.91 eV (5.75 eV) in PBE, and 2.39 eV (5.34 eV) in PBE + U, respectively. The calculated 2p-5f/6d gap of ThO_2 is 4.47 eV (4.81 eV) in the PBE (PBE + U) calculation. The calculated ground-state band gaps are slightly smaller than experimental values, but in accordance with other DFT and DFT + U calculations.[6,9,10,18,36,37] Considering that electronic bands broaden greatly at high pressures, we can expect an insulator-metal transition in CeO_2 and ThO_2. The transition mechanism of course should be the Wilson type, i.e., via band broadening and overlapping. Figure 8 shows the pressure dependence of the calculated band gaps in CeO_2 and ThO_2, with PBE and PBE + U functionals, respectively. The $P\bar{3}m1$ and $I4/mmm$ phases in CeO_2 are always metallic and not presented here. We see that both PBE and PBE + U calculations gave similar results. The predicted metallization pressure in CeO_2 is about 250 GPa, whereas in ThO_2 it is around 350 GPa.

In order to justify the predicted metallization mechanism of Wilson transition, Fig. 9 demonstrates the total and projected DOS (PDOS) of the LP-$Pnma$ phase and those of the HP-$Pnma$ phase in CeO_2 at around its metallization pressures. The scenario in ThO_2 is similar and not shown here. We can see that there is significant broadening and overlapping between the predominantly O-2p featured valence band and the Ce-5f conduction band. The bandwidth of the O-2p valence band broadens to 10 eV at 250 GPa, compared to 4 eV in the fluorite phase at zero pressure, and 5 eV at the pressure of fluorite-cotunnite transition. The 5f and 6d states of the conduction bands also broaden greatly.

It should be pointed out that the DOS at the Fermi level is rather small for a wide pressure range above the metallization pressures, indicating that CeO_2 and ThO_2 might be semimetals

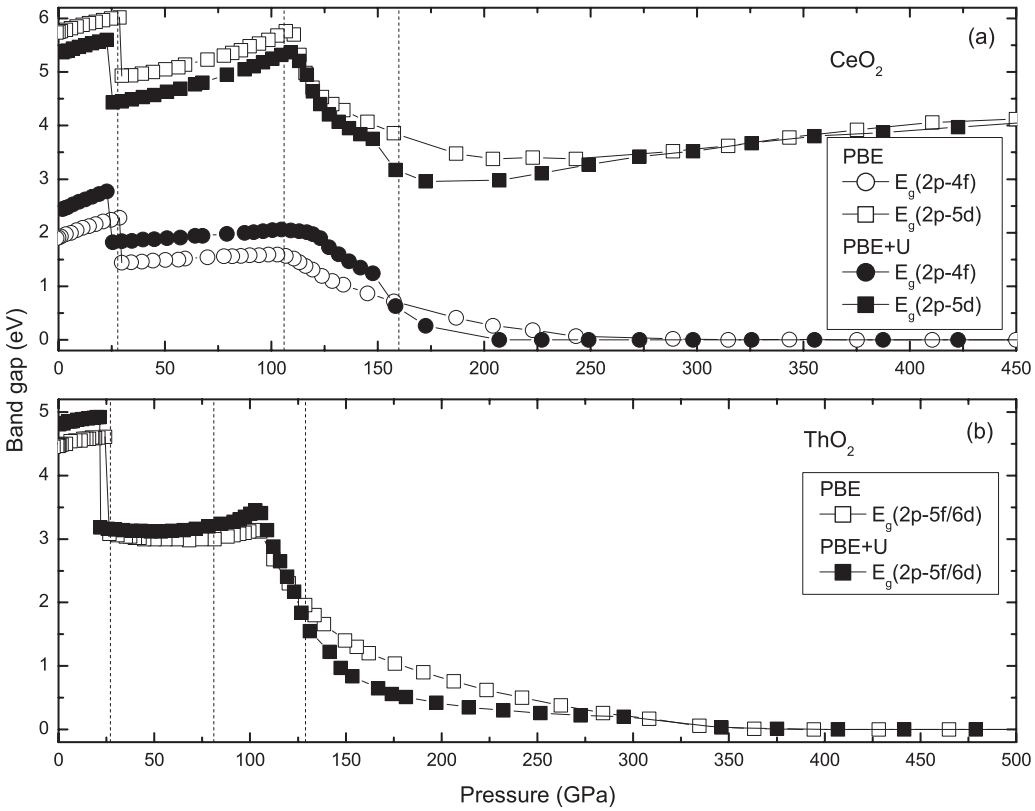

FIG. 8. Pressure dependence of the band gap E_g for (a) CeO_2 and (b) ThO_2. Dashed lines denote the isostructural transition zones within space group *Pnma* and the transition pressures from fluorite to cotunnite, calculated with PBE functional.

or gapless semiconductors. This feature was also observed in PuO_2 when above 123 GPa.[41] Nevertheless, the mechanisms of pressure-induced metallization in CeO_2, ThO_2, UO_2, and PuO_2 are different: it is a Wilson transition in CeO_2 and ThO_2, whereas in UO_2 it is a Mott transition, and in PuO_2 a Peierls transition. Furthermore, in CeO_2, ThO_2, and UO_2, the transition belongs to the second order, but in PuO_2 it is a first-order transition.[41] Instead of the semimetal-like behavior around the metallization pressures, the DOS at the Fermi level in the $P\bar{3}m1$ and $I4/mmm$ phases of CeO_2 are much larger, namely, a behavior of normal metals.

As shown in Fig. 8, the variation of the band gaps under compressions in CeO_2 or ThO_2 is different from that of UO_2 or PuO_2.[41] In the fluorite phase, the change of band gaps in CeO_2 and ThO_2 is increasing with pressure, due to ascending of the unoccupied Ce-4f and Th-5f/6d conduction bands against the Fermi level. By contrast, the band gap decreases with pressure in UO_2, and keeps almost constant in PuO_2. At the fluorite-cotunnite transition point, the band gaps suddenly decrease in CeO_2 and ThO_2, whereas in UO_2 and PuO_2 they slightly increase. This difference might originate from their insulating nature. As mentioned above, in CeO_2 and ThO_2, the top of the valence band is predominantly anions p featured (with a hybridization with f orbitals), and the bottom of the conduction band is mainly cations f featured. In other words, they belong to charge-transfer insulators. Instead, UO_2 is a typical Mott-Hubbard insulator, while PuO_2 lies in an intermediate region between the Mott-Hubbard insulator and charge-transfer insulator.[41] Therefore the change of the band gap in UO_2 and PuO_2 is mainly determined by the correlation effects of the f orbitals, whereas in CeO_2 and ThO_2 the dispersion of the fully delocalized orbitals governs how the band gap varies.

In the cotunnite phase of CeO_2, the 2p-4f gap increases slowly with pressure; in contrast, the 2p-5d gap increases much more rapidly. This is because the ascending of the Ce-5d conduction band is more significant than that of the Ce-4f band. Such change in the cotunnite phase of ThO_2 is not prominent and the variation of its 2p-5f/6d gap is much smaller than in CeO_2. Within the transition zones, the broadening of the valence and conduction bands is the main feature, leading all gaps in CeO_2 and ThO_2 to decrease rapidly with pressure. The 2p-4f gap in CeO_2 and the 2p-5f/6d gap in ThO_2 decrease continuously to zero, while the 2p-5d gap of CeO_2 rebounds in the HP-*Pnma* phase, implying a different behavior of the d orbitals in these two compounds. However, after transition into the metallic $P\bar{3}m1$ phase of CeO_2, the 2p-5d gap also vanishes.

The bonding properties of these high-pressure phases were also investigated. Remarkably, we found that there are quite unexpected covalent bonds between the Ce cations, which arises from the hybridization of p orbitals. Figure 10 shows the differential charge density along the [001] plane, calculated with PBE functional. The charge accumulation between the nearest Ce cations is evident. It is worth mentioning that the nearest Ce-Ce distance is 2.32 Å, which is much larger than the nearest distances of Ce-O (1.87 Å) and O-O (1.86 Å). This observation indicates that the interactions of Ce-Ce and O-O

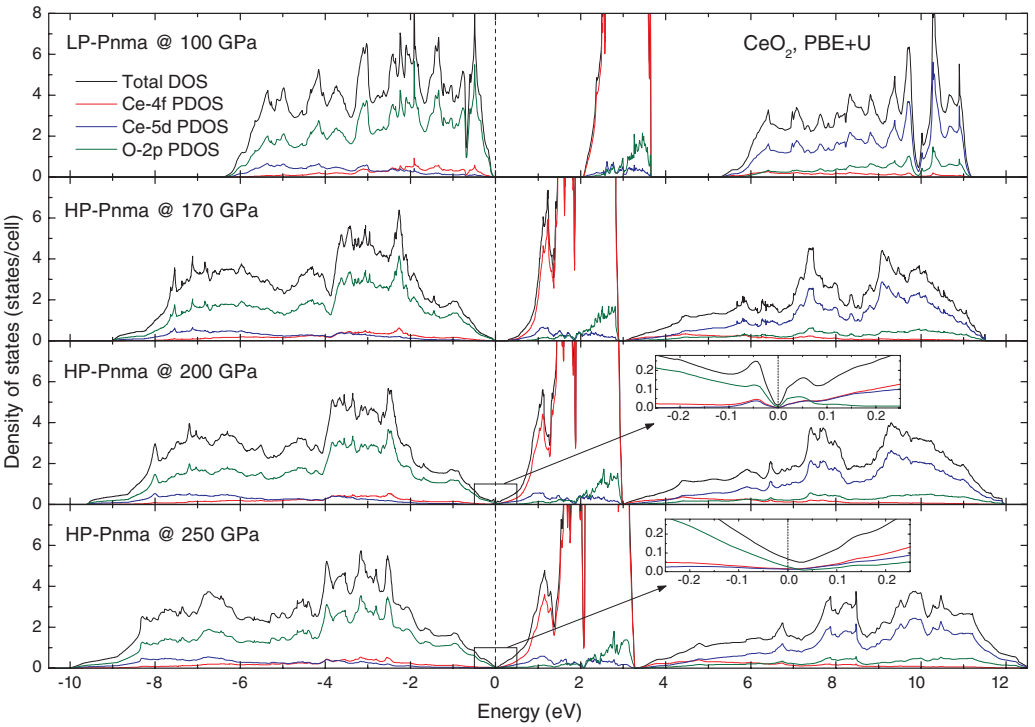

FIG. 9. (Color online) Total and projected electronic density of states for CeO_2 calculated by PBE + U at selected pressures. Insets show the enlarged regions around the Fermi levels, which are denoted by dashed lines. Band broadening and overlapping are evident.

take an important role to stabilize the $I4/mmm$ phase, which might be in a comparable magnitude as the contribution from cation-anion interactions. Furthermore, although the nearest O-O distance is still much larger than the bond length of O_2 molecule at ambient conditions (1.21 Å, see Ref. 51), formation of a stretched O_2 dimer might be possible at higher pressures, on the condition that CeO_2 is still chemically stable.

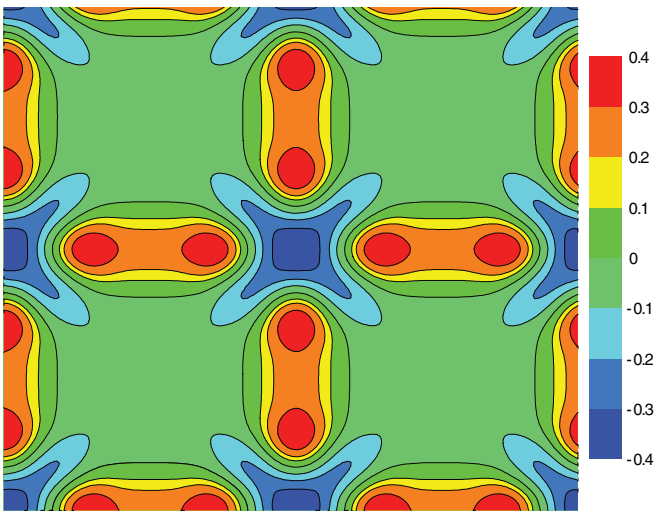

FIG. 10. (Color online) Calculated differential charge density on the [001] plane of a 2 × 2 × 1 supercell of the $I4/mmm$ phase in CeO_2 at 850 GPa. This plane contains only the metal cations, which locate at the center of small dark blue regions. The unexpected covalent bonds between Ce atoms are evident.

IV. CONCLUSIONS

We studied the high-pressure structural and electronic behaviors of CeO_2 and ThO_2, up to 1 TPa. The isostructural transition within space group $Pnma$ in CeO_2 and ThO_2 was investigated. We identified the high-pressure $Pnma$ phase as an orthorhombic distortion of the hexagonal Ni_2In structure with space group $P6_3/mmc$. It seems that the postcotunnite phases in actinide dioxides and lanthanide dioxides all have a close relationship with the hexagonal Ni_2In structure, namely, the $Cmc2_1$ distortion in UO_2, $Cmcm$ distortion in PuO_2, and $Pnma$ distortion in CeO_2 and ThO_2. The high-pressure $Pnma$ phase is also responsible for the pressure-induced metallization in CeO_2 and ThO_2, at about 250 and 350 GPa, respectively. The underlying physical mechanism belongs to the Wilson transition. Furthermore, two new ultrahigh-pressure metallic phases with space group $P\bar{3}m1$ and $I4/mmm$ were found being stable between 450 GPa and 1 TPa in CeO_2. The similarities and/or differences among CeO_2, ThO_2, UO_2, and PuO_2 were elaborated in terms of the structural and electronic properties. Considering that CeO_2 is widely used as a nonradioactive surrogate material for nuclear fuel UO_2 and PuO_2, our results will be helpful for further investigations on these technical materials.

ACKNOWLEDGMENTS

Support by the Industrial Technology Development Program under Grant No. B1520110001, the Fund of National Natural Science Foundation of China under Grant No. 11274281, and the Foundation for Development of Science and Technology of CAEP under Grant No. 2012A0101001, is acknowledged.

*Author to whom correspondence should be addressed: huay.geng@gmail.com

[1] G. A. Kourouklis, A. Jayaraman, and G. P. Espinosa, Phys. Rev. B **37**, 4250 (1988).

[2] S. J. Duclos, Y. K. Vohra, A. L. Ruoff, A. Jayaraman, and G. P. Espinosa, Phys. Rev. B **38**, 7755 (1988).

[3] A. Jayaraman, G. A. Kourouklis, and L. G. Van Uitert, Pramana J. Phys. **30**, 225 (1988).

[4] J. P. Dancausse, E. Gering, S. Heathman, and U. Benedict, High Press. Res. **2**, 381 (1990).

[5] M. Idiri, T. LeBihan, S. Heathman, and J. Rebizant, Phys. Rev. B **70**, 014113 (2004).

[6] C. Sevik and T. Çağın, Phys. Rev. B **80**, 014108 (2009).

[7] N. V. Skorodumova, R. Ahuja, S. I. Simak, I. A. Abrikosov, B. Johansson, and B. I. Lundqvist, Phys. Rev. B **64**, 115108 (2001).

[8] L. Petit, A. Svane, Z. Szotek, and W. M. Temmerman, Phys. Rev. B **72**, 205118 (2005).

[9] J. L. F. Da Silva, M. V. Ganduglia-Pirovano, J. Sauer, V. Bayer, and G. Kresse, Phys. Rev. B **75**, 045121 (2007).

[10] C. Loschen, J. Carrasco, K. M. Neyman, and F. Illas, Phys. Rev. B **75**, 035115 (2007).

[11] E. Wuilloud, B. Delley, W. D. Schneider, and Y. Baer, Phys. Rev. Lett. **53**, 202 (1984).

[12] E. T. Rodine and P. L. Land, Phys. Rev. B **4**, 2701 (1971).

[13] Z. Wang, S. K. Saxena, V. Pischedda, H. P. Liermann, and C. S. Zha, Phys. Rev. B **64**, 012102 (2001).

[14] S. Rekhi, S. K. Saxena, and P. Lazor, J. Appl. Phys. **89**, 2968 (2001).

[15] S. Mehrotra, P. Sharma, M. Rajagopalan, and A. Bandyopadhyay, Solid State Commun. **140**, 313 (2006).

[16] S. Li, R. Ahuja, and B. Johansson, High Press. Res. **22**, 471 (2002).

[17] J. C. Boettger, Int. J. Quantum Chem. **109**, 3564 (2009).

[18] B. T. Wang, H. Shi, W. D. Li, and P. Zhang, J. Nucl. Mater. **399**, 181 (2010).

[19] H. Y. Geng, Y. Chen, Y. Kaneta, and M. Kinoshita, Phys. Rev. B **75**, 054111 (2007).

[20] P. Hohenberg and W. Kohn, Phys. Rev. **136**, B864 (1964).

[21] W. Kohn and L. J. Sham, Phys. Rev. **140**, A1133 (1965).

[22] G. Kresse and J. Furthmüller, Phys. Rev. B **54**, 11169 (1996).

[23] G. Kresse and J. Furthmüller, Comput. Mater. Sci. **6**, 15 (1996).

[24] J. P. Perdew, K. Burke, and M. Ernzerhof, Phys. Rev. Lett. **77**, 3865 (1996).

[25] P. E. Blöchl, Phys. Rev. B **50**, 17953 (1994).

[26] G. Kresse and D. Joubert, Phys. Rev. B **59**, 1758 (1999).

[27] P. E. Blöchl, O. Jepsen, and O. K. Andersen, Phys. Rev. B **49**, 16223 (1994).

[28] H. J. Monkhorst and J. D. Pack, Phys. Rev. B **13**, 5188 (1976).

[29] V. Kanchana, G. Vaitheeswaran, A. Svane, and A. Delin, J. Phys.: Condens. Matter **18**, 9615 (2006).

[30] T. Gürel and R. Eryiğit, Phys. Rev. B **74**, 014302 (2006).

[31] Z. Yang, T. K. Woo, M. Baudin, and K. Hermansson, J. Chem. Phys. **120**, 7741 (2004).

[32] P. J. Hay, R. L. Martin, J. Uddin, and G. E. Scuseria, J. Chem. Phys. **125**, 034712 (2006).

[33] J. Kullgren, C. W. M. Castleton, C. Müller, D. M. Ramo, and K. Hermansson, J. Chem. Phys. **132**, 054110 (2010).

[34] S. Fabris, S. de Gironcoli, S. Baroni, G. Vicario, and G. Balducci, Phys. Rev. B **71**, 041102(R) (2005).

[35] Y. Jiang, J. B. Adams, and M. van Schilfgaarde, J. Chem. Phys. **123**, 064701 (2005).

[36] D. A. Andersson, S. I. Simak, B. Johansson, I. A. Abrikosov, and N. V. Skorodumova, Phys. Rev. B **75**, 035109 (2007).

[37] J. J. Plata, A. M. Márquez, and J. F. Sanz, J. Chem. Phys. **136**, 041101 (2012).

[38] H. Jiang, R. I. Gomez-Abal, P. Rinke, and M. Scheffler, Phys. Rev. Lett. **102**, 126403 (2009).

[39] S. L. Dudarev, G. A. Botton, S. Y. Savrasov, C. J. Humphreys, and A. P. Sutton, Phys. Rev. B **57**, 1505 (1998).

[40] Y. Wang, J. Lv, L. Zhu, and Y. Ma, Phys. Rev. B **82**, 094116 (2010).

[41] H. X. Song, H. Y. Geng, and Q. Wu, Phys. Rev. B **85**, 064110 (2012).

[42] *International Tables for Crystallography, Volume A1: Symmetry Relations Between Space Groups*, edited by H. Wondratschek and U. Müller (Kluwer, Dordrecht, 2004).

[43] U. Müller, *Symmetry Relations Between Crystal Structures*, Summer School on Mathematical and Theoretical Crystallography, 27 April–3 May 2008, Gargnano, Italy.

[44] P. Zhang, B. T. Wang, and X. G. Zhao, Phys. Rev. B **82**, 144110 (2010).

[45] D. Santamaría-Pérez, A. Vegas, C. Muehle, and M. Jansen, J. Chem. Phys. **135**, 054511 (2011).

[46] G. Henkelman, A. Arnaldsson, and H. Jónsson, Comput. Matter. Sci. **36**, 254 (2006).

[47] E. Sanville, S. D. Kenny, R. Smith, and G. Henkelman, J. Comput. Chem. **28**, 899 (2007).

[48] W. Tang, E. Sanville, and G. Henkelman, J. Phys.: Condens. Matter **21**, 084204 (2009).

[49] L. Gerward, J. S. Olsen, L. Petit, G. Vaitheeswaran, V. Kanchana, and A. Svane, J. Alloys Compd. **400**, 56 (2005).

[50] L. Liu, H. X. Song, Z. Wang, H. Y. Geng, Q. Jing, Y. Zhang, S. Liu, S. Xiang, Y. Bi, J. Xu *et al.*, J. Appl. Phys. **112**, 013532 (2012).

[51] K. P. Huber and G. Herzberg, *Constants of Diatomic Molecules* (Van Nostrand, New York, 1979).